Water Confinement in Hydrophobic Nanopores. Pressure-Induced Wetting and Drying

Sergei Smirnov,* Ivan Vlassiouk,† Pavel Takmakov,‡ and Fabian Rios

Department of Chemistry and Biochemistry, New Mexico State University, Las Cruces, New Mexico 88003. †Current address: Oak Ridge National laboratory, Oak Ridge, Tennessee 37831. ‡Current address: Department of Chemistry, University of North Carolina at Chapel Hill, Chapel Hill, North Carolina 27599.

ABSTRACT Wetting and drying of hydrophobic pores with diameters lower than 0.2 μm by aqueous solutions at different hydrostatic pressures is investigated by measuring the ionic conductance variation through the nanopores. The critical pressure for water intrusion into the nanopores increases with lowering the pore diameter and the surface tension of the hydrophobic modification, in agreement with the Laplace equation. Nevertheless, restoring the pressure to the atmospheric one does not result in spontaneous pore dewetting unless bubbles are left inside the pores. Such bubbles can appear at the regions of narrowing cross section and/or varying quality of the hydrophobic modification and thus can be engineered to control water expulsion.

KEYWORDS: hydrophobicity · ionic conductance · nanopores · spontaneous dewetting

Investigation and utilization of hydrophobic surfaces for various applications has gained a new momentum recently. Hydrophobicity is a fundamental property that controls interactions between nonpolar substances and water. These interactions in turn are responsible for numerous physical and biophysical phenomena. Hydrophobicity has been studied extensively, but many aspects are still not well understood. Strong attraction between water molecules due to hydrogen bonding makes their interaction with nonpolar substances unfavorable. Poor wetting of a hydrophobic surface by water can be observed experimentally as a large contact angle between a water droplet and the surface.

Recent development of nanometer scale systems and their applications in the biological, chemical, and physical sciences increasingly emphasizes the importance of interfaces: the smaller the object size, the greater its surface-to-volume ratio. What could have been an insignificant annoyance in the macroscopic and even microscopic systems can no longer be ignored on the nanoscale. Behavior of a liquid near the solid surface is substantially different from that in the bulk and is affected by confinement of liquid in nanosized voids. Water at a hydrophilic surface was predicted by computer simulation to have a higher density than in the bulk,[1] while near hydrophobic surfaces, a thin layer of low-density water is expected.[1−5] Another striking theoretical prediction is that water confined between two hydrophobic surfaces or in a hydrophobic pore is supposed to spontaneously evaporate when the size of the pore is sufficiently small.[3−5] Since the phenomenon is important fundamentally as well as to various applications such as electrowetting[6] and sensors,[7] it is essential to identify the conditions when spontaneous evaporation can occur.

Similarly to the interior of biological membranes, artificial membranes can be made hydrophobic and impermeable to water and dissolved in it ions. Moreover, the hydrophobic surface can be also made responsive to various stimuli that switch its surface tension[7−9] and turn the membrane into an artificial mediator for transport of ions and other species. In living organisms, such transfer across the membrane is selective and controls a variety of metabolic and signaling purposes, such as nerve impulses generated by the controlled release of ions across the membranes. Mimicking biological channels using synthetic nanopores is a challenging scientific problem with possible applications in medicine, materials science, fuel cells, analytical chemistry, and sensors. We recently showed that such switching can be initiated by light in the membrane's surface of which is modified by a mixed monolayer of hydrophobic molecules and photochromic spiropyran[8] or by pH in hydrophobic membranes with amino or carboxyl groups.[10] In order to have a full control of the nanopore wetting, one desires to have the switching capability in

*Address correspondence to snsm@nmsu.edu.

Received for review May 17, 2010 and accepted July 30, 2010.

Published online August 6, 2010. 10.1021/nn101080k

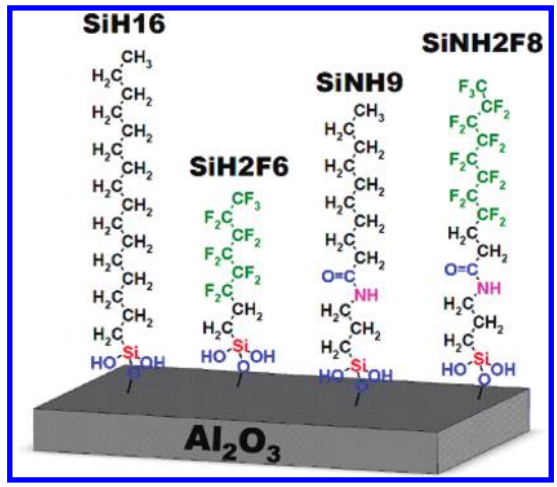

Figure 1. Four types of hydrophobic surface modifications used in this study with their labels. The first two (SiH16 and SiH2F6) were obtained using toluene solutions of hexadecyltrimethoxysilane and 1*H*,1*H*,2*H*,2*H*-perfluorooctyltrichlorosilane, respectively. The last two (SiNH9 and SiNH2F8) were obtained in two steps: first "amination" using aminopropyl trimethoxysilane in toluene, and then reaction with either decanoic acid or fluoroundecanoic acid using EDC coupling reagent in ethanol. For simplicity, Si atoms are drawn connected to the surface *via* a single Si−O bond; the remaining two bonds are presented as hydroxyls, but at high densities, most neighboring silanes form lateral Si−O−Si bonds.

both directions, from dry to wet and in reverse. The reverse transition is what we address in this paper.

Here we describe the investigation of spontaneous dewetting in hydrophobic nanoporous membrane filters using electrical impedance measurements. Understanding this phenomenon should provide insight into the behavior of hydrophobic nanopores and offers practical implications for utilization of natural and artificial systems with tailored responsive hydrophobic/hydrophilic surface properties. We demonstrate that spontaneous dewetting of hydrophobic nanopores can occur only when the pores are not completely filled with water/electrolyte. When monitored electrically, the effect appears as a significant but incomplete recovery of the ionic resistance through membrane after dewetting. No recovery of the resistance is observed when the pores are filled with water completely. The incomplete recovery is due in part to hysteresis of the surface conductance.

RESULTS AND DISCUSSION

The membranes were modified with aliphatic and fluorinated silanes, as shown in Figure 1 and described in Materials and Methods, to make them highly hydrophobic. An apparent contact angle for a small water drop (in the sessile technique) is greater than 140° for all of them. Despite no electrolyte intrusion into the membrane at ambient external pressure, membranes have very low but measurable conductance that depends on the modifier and not on the electrolyte concentration or its pH.[13] Membranes with these hydrophobic modifiers show very high resistance, greater than 1 MΩ, and remain superhydrophobic for indistinguishably long time if left in electrolyte. Their resistance varies in the following order: SiH16 > SiNH2F8 > SiNH9, which was discussed previously,[13] and is due to surface conductance from ionizable groups below the hydrophobic monolayer. Residual hydroxyls on alumina surface and on silanes as well as amines and amides of the linkers contribute to that surface conductance. Their hydration and the resulting conductance were found to slightly increase over time, which is also related to hysteresis of the contact angle. Autoionization of residual water bound on the surface contributes to the effect, as well.

The fact that the resistance is not infinite allows one to use it for monitoring the extent of water/electrolyte intrusion into the pores. In a simple model that we previously discussed,[13] the resistance of a single pore with constant diameter, D, and length L, is given by

$$R_{\text{pore}} = R_s \frac{L}{\pi D} \tag{1}$$

where R_s is the sheet resistance of the hydrophobic monolayer. If the pore is partially filled with electrolyte, the resistance of that portion is insignificant (by many orders of magnitude) as compared to the surface wall resistance of the "dry" portion. Thus one can still use eq 1 in this case with L referring to the length of the dry portion.

The equilibrium of forces at a water−gas interface in a nanopore can be described by balancing the pressure difference with the capillary force:

$$\Delta P = P_{\text{ext}} - P_{\text{in}} = -\Delta\gamma\left(\frac{1}{r_1} + \frac{1}{r_2}\right) \tag{2}$$

where r_1 and r_2 are the curvatures of meniscus at the pore mouth, P_{ext} is the external pressure on the outside of the membrane, and P_{in} is the pressure inside the pore. By virtue of how the cell is prepared in our experiments, P_{in} always equals the vapor pressure of water, $P_{\text{in}} = P_{\text{vap}}$ (~23 Torr at 25 °C). The surface tension difference, $\Delta\gamma$, between the wall/vapor, γ_{wv}, and wall/liquid, γ_{wl}, interfaces relates to the surface tension of the free liquid−vapor interface, γ, and the contact angle, θ, on the surface *via* the Young equation:

$$\Delta\gamma \equiv \gamma_{\text{wv}} - \gamma_{\text{wl}} = \gamma\cos\theta \tag{3}$$

For a hydrophilic surface ($\theta < 90°$), the equilibrium in eq 2 cannot be sustained at any external pressure (since $P_{\text{ext}} \geq P_{\text{vap}}$) and water fills up the pore. For a hydrophobic surface ($\theta > 90°$), the pore remains dry until the external pressure reaches its critical value, which is dependent on $\Delta\gamma$ and the pore cross section. The latter can be mimicked as an ellipse with the two diameters, D_1 and D_2, which become identical for a perfectly cylindrical pore $D = D_1 = D_2$. The critical pressure for

nanometer-sized pores is usually much higher than the water vapor pressure, which allows neglecting P_{in} in eq 2. The pressure, ΔP_o, at which water is capable of intruding into the pores[15]

$$P_o \approx \Delta P_o = -2\gamma \cos\theta_a\left(\frac{1}{D_1} + \frac{1}{D_2}\right) \quad (4)$$

is quite large even for the largest pores in our study. Indeed, for uniform diameter $D = 0.2$ μm and hydrophobic modification of a modest advancing contact angle of $\theta_a \sim 105°$ (*i.e.*, $|\Delta\gamma| \sim 19$ mN/m), the critical pressure is $\Delta P_o \sim 3.8$ bar. Simple electrolytes, such as KCl used here, have minimal effect on the surface tension. According to ref 16, 1.0 M KCl solution has γ only insignificantly increased from 72 to 74 mN/m. Thus, the outcome of measurements with 1.0 M KCl can be presumed to hold almost identically to such with pure water.

The pores in the membrane are not identical; they vary in the quality of coverage (*i.e.*, different $\Delta\gamma$) and the pore diameter that fluctuates not only between the pores but likely within the pore as well, as is illustrated by Figure 2. From SEM images, "0.2 μm" Whatman membranes have an average 213 nm diameter on one side and 114 nm on the other side.[11] From the porometry measurements,[11] one side of these membranes has pore diameters, D, ranging from 122 to 256 nm (with 143 nm at 50% level) and another side from 130 to 178 nm (with 152 nm at 50% level). As a result, the water intrusion into the membrane happens not at a single pressure but over a range of pressures.

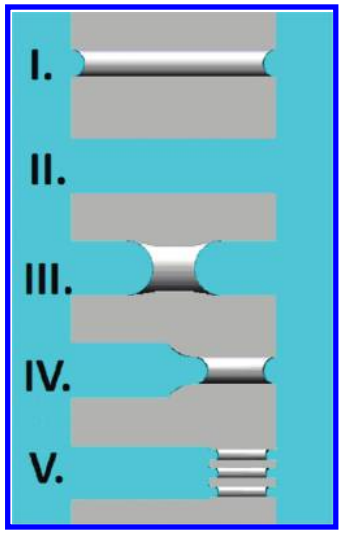

Figure 2. Illustration of different pore morphologies in a membrane with hydrophobic modification and their response to hydrostatic pressure of water (blue) that is insufficient to intrude into pores of a too small diameter (I) but penetrates through large pores (II). Pores with variable diameter (III and IV) have incomplete water penetration. Type III has uncontrolled (unintentional) diameter variation, while type IV is often realized for alumina membranes that are not "perfectly open" after their construction using anodization of Al. Type V represents the geometry of commercial 0.02 μm membranes from Whatman, where the 0.02 μm portion is only 1 μm deep on one side of the membrane and its remaining 59 μm of thickness has pores with the nominal 0.2 μm diameter.[11]

Figure 3 demonstrates the variation of the resistance as a function of pressure for the two types of commercial membranes, 0.2 and 0.02 μm, with two types of hydrophobic surface modifications. Comparison of 0.2 μm membranes with SiH16 and SiNH2F8 modifications reveals that both demonstrate a broad range of pressures when water intrudes into the membrane and causes the resistance to decline. The ratio of the highest to the lowest pressure is roughly a factor of 2, in agreement with the pore diameter distribution.[11] At the same time, the SiNH2F8-modified membrane requires almost twice as much pressure to become totally open, more than 12 bar *versus* just 7 bar for the SiH16 membrane. These values are in a good agreement with the contact angles on flat surfaces of $\theta_a \sim 105$ and 120° for surfaces modified with SiH16 and SiNH2F8, respectively, and the pore diameter *ca.* 120 nm is the smallest pore diameter for such membranes.[11] Incidentally, the low limit pressures in both cases are roughly half the highest value, in agreement with the higher end values in the pore diameter distribution (*ca.* 250 nm).

After reaching the critical pressure, when the membrane resistance equals the value corresponding to it being filled with electrolyte (*ca.* 17 Ω), the resistance remains this low even after the pressure is reduced to the atmospheric one. This is a relatively well-understood situation,[5] where spontaneous dewetting of hydrophobically modified nanopores is kinetically unfeasible despite the significant thermodynamic advantage. A high activation barrier makes such a transition kinetically impossible for the nanopore diameters greater than $D > 10$ nm. The transition state requires formation of a bubble inside the pore, which defines a large activation barrier, $\Delta\Omega^{\#}$. From the standard capillary theory, the latter can be estimated by analyzing the grand potential variation, $\Delta\Omega$, upon creation of a vapor bubble of volume V_V that has a surface area S_{SV} in contact with the walls and S_{LV} area of the liquid/vapor interface:[17,18]

$$\Delta\Omega = V_V\Delta P + S_{LV}\gamma_{lv} + S_{SV}(\gamma_{sv} - \gamma_{sl}) = V_V\Delta P + S_{LV}\gamma + S_{SV}\gamma\cos\theta \quad (5)$$

The two types of transition states, a cylindrically symmetric annular doughnut-like void and a bubble on the wall, have similar activation barriers that scale approximately as the pore diameter squared, D:[17]

$$\Delta\Omega^{\#} \approx \pi\gamma D^2(A + B\delta) \quad (6)$$

The dimensional parameter $\delta = D\Delta P/4\gamma$ is an effective measure of the relative contributions from the surface tension and the vapor expansion terms. The coefficients A and B differ for the two cases of transition states and depend on the contact angle, but both are on the order of unity (actually, they are less than 1[17]). Equation 6 sug-

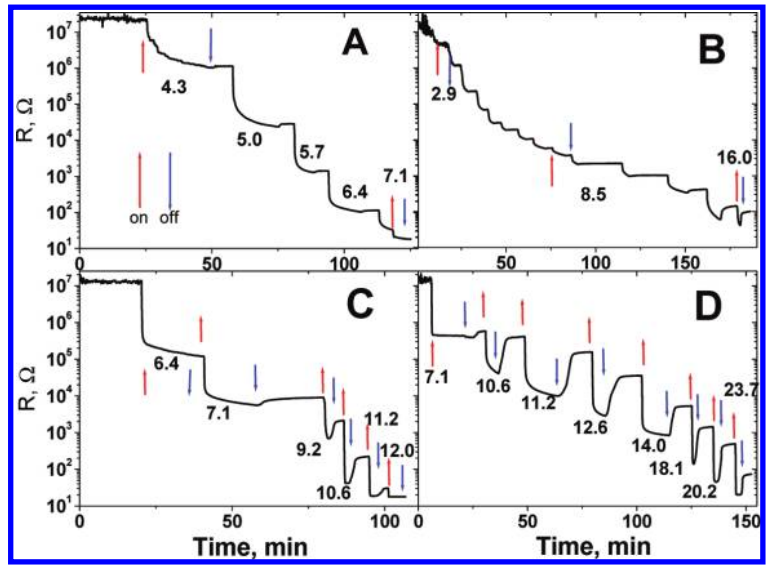

Figure 3. Variation of the impedance at 100 Hz with hydrostatic pressure for commercial 0.2 and 0.02 μm membranes modified with SiNH2F8 and SiH16. Arrows indicate the points when pressure was increased (up) to a designated value in bars and decreased (down) to the atmospheric pressure, respectively. (A) 0.2 μm membrane modified with SiH16. Pressure steps are 0.7 bar starting with 4.3 bar. (B) 0.02 μm membrane modified with SiH16. Pressure steps are 0.7 bar (from 2.9 to 8.5 bar) and 1.5 bar (from 8.5 to 16.0 bar). Every step of the pressure increase is followed by discharge to the atmospheric pressure (~0.9 bar). (C,D) 0.2 and 0.02 μm membranes modified with SiNH2F8.

gests that for $D \sim 150$ nm the activation barrier is extremely high, $\Delta\Omega^{\#} > 10^6\ k_BT$, and bubbles cannot spontaneously form in a reasonable time. Even for $D \sim 20$ nm, the barrier is too high, $\Delta\Omega^{\#} > 2 \times 10^4\ k_BT$. Additional contribution to $\Delta\Omega^{\#}$ in eq 5 from line tension that is proportional to the length of the three phase separation line can somewhat lower[17] $\Delta\Omega^{\#}$, but it would still be insufficient to increase the probability of bubble formation to a measurable value for the pores of $D > 10$ nm.

The situation at intermediate pressures is less obvious. When the applied pressure is restored down to the atmospheric one, the membrane resistance partially recovers. The extent of this recovery is negligible with SiH16 modifier (Figure 3A), but it can reach as much as 15% with SiNH2F8 (Figure 3B) at pressures near 8−9 bar, which correspond to the maximum in the pore distribution by diameters (~150 nm). Distribution of pore diameters causes water intrusion at different pressures, and the type of this distribution affects the manner in how it proceeds. Uneven pore diameter also affects the recovery after the external pressure drops to the atmospheric one. If the pores are perfect cylinders but of different diameters, then they should be entirely filled with water as soon as the critical pressure of eq 4 is reached. Large pores are filled first and the smallest pores last, as illustrated by cases I and II in Figure 2. Pores entirely filled with water do not dry out after the pressure is dropped back to the atmospheric one due to the above mentioned large activation barrier.

A pore with variable diameter (such as in the cases III and IV of Figure 2), say from D_{min} to D_{max}, may end up at a pressure that exceeds the critical P_o for D_{max} but too low for penetrating into the narrowing of D_{min}. The electrical resistance of the pore at such pressure would significantly decrease in accordance with a shorter vapor gap but would still be large since the conductance through the gap portion is very small. This vapor gap helps in spontaneous pore dewetting after releasing the pressure. Water is pushed out of the pore by the surface tension at the interface with vapor and the walls as long as the contact angle with the surface stays above 90°. For high-quality surface modifications, the contact angle remains almost unaffected by history of its exposure, but for rough and/or inhomogeneous surfaces, the hysteresis of the contact angle (the difference between the advancing, θ_a, and receding, θ_r, angles) can be as high as 10−15°. For aliphatic surface modifiers, it can cause the receding contact angle to fall below 90°, that is, when spontaneous dewetting would not be possible for cylindrical pores. The receding contact angle for fluorinated surfaces, even with large hysteresis, remains above 90°, which can explain the difference in behavior of SiNH2F8 and SiH16 0.2 μm membranes. Inhomogeneity of hydrophobic surface modification broadens the distribution of critical pressures P_o and the extent of recovery after the pressure release.

Besides the narrowing in the pores, such as in the case III, other imperfections can also appear during membrane preparation. The pores grown by anodization of metallic Al foil are sealed on one side and need additional chemical (with phosphoric acid), electrochemical (changing the anodization voltage at the end), mechanical (polishing), or a combination of such means to eliminate the oxide barrier on one side, that is, to make them opened. Depending on the process, the re-

sulting diameters can vary significantly, and for Whatman 0.2 μm membranes, it was shown to have different distributions of diameters on the two sides of the membranes.[11]

To confirm the interpretation and further illustrate the importance of bubbles for spontaneous dewetting of pores filled with water, we repeated experiments with the homemade membranes of the nominal pore diameter 70 nm and with 0.02 μm membranes from Whatman (Figures 3B,D and 4). Smaller pore diameters translate into larger pressures required for water intrusion, and a narrower distribution by diameters should similarly correspond to a narrower range of critical pressures.

Homemade membranes have been prepared under much better controlled conditions, which results in a more circular shape of the pores and a narrower distribution of their diameters, around 70 nm. However, the way the pores were "opened" (by the phosphoric acid treatment) could likely cause their uneven widening from the original 50 nm diameter (before the treatment) to 70 nm.

The smaller pore diameters of 70 nm indeed result in a larger pressure for complete water intrusion, almost by a factor of 2 (see Figure 4), in agreement with the factor of 2 in the diameter decrease as compared with the 0.2 μm membrane. The narrower distribution of pore diameters in the homemade 70 nm membrane modified with SiNH2F8 also illustrates a significant narrowing of the critical pressure range, as compared with 0.2 μm membranes. As seen in the logarithmic plot of the inset of Figure 4, less than 0.1% of the pores are filled with water before the last step of pressure increase, which is a remarkably narrow distribution as compared to that of the 0.2 μm membrane. Additional breadth to both distributions is brought by the non-uniformity of surface modification, which results in a distribution of surface energies (contact angles). Note that the resistance recovery upon pressure dropping is similarly smaller for the homemade membrane.

The so-called 0.02 μm membranes from Whatman actually have the same ~150 nm (0.2 μm nominal) diameter throughout 59 μm of their total 60 μm thickness, and only the remaining 1 μm on one side has the nominal diameter 0.02 μm, as was previously described[19] and is sketched as the case V in Figure 2. It is not as important in this case that the 0.02 μm side has a broad distribution of the pore diameters with the average diameter exceeding 20 nm, but it is essential that these pores are noticeably *smaller* and connected with 0.2 μm pores. The difference in diameters assures the existence of a wide range of pressures when water can intrude only into the 0.2 μm part and leave the 0.02 μm side dry. It also means that the condition when pores should be able to spontaneously dry out upon release of excess pressure can be satisfied.

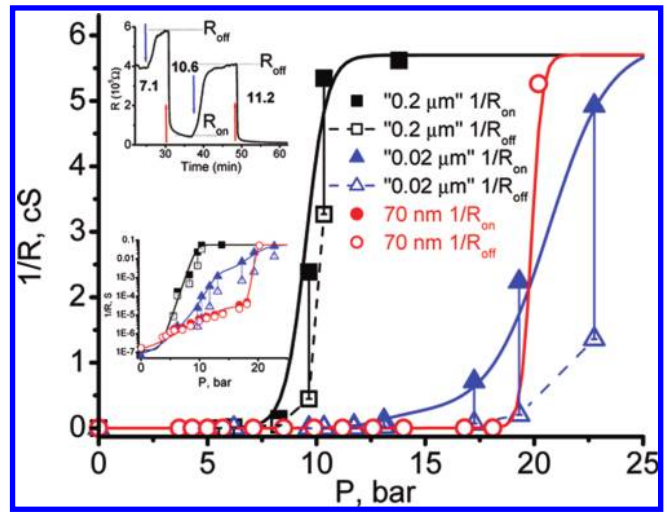

Figure 4. Pressure dependence of the conductance for hydrophobic membranes of Figure 3 and for the fluorinated 70 nm pore diameter membrane. Two points for each pressure represent values at that pressure (filled) and after its releasing back to the atmospheric one (empty). Squares illustrate the 0.2 μm membrane, triangles the 0.02 μm membrane, and circles −70 nm. The bottom inset shows the same graph in linear scale. The top inset illustrates the labeling of resistances using a portion of the graph in of Figure 3D: when the pressure is applied (10.6 bar in this case), R_{on}, and upon recovery to the atmospheric pressure, R_{off}.

Figures 3 and 4 confirm that the 0.02 μm membrane with SiNH2F8 modification does require very high pressure for complete water intrusion. Even the highest experimentally available pressure of 23 bar is not sufficient to achieve total wetting of the membrane. A noticeable change of resistances is observed in a broader range of pressures, as expected for a much broader distribution of pore diameters. More noticeable is significantly improved resistance recovery, especially in the range of pressures below 11 bar, where it reaches up to 70%. Since now the pore diameter variation resembles that of the case V in Figure 2, water does not occupy the pores completely upon intrusion, and the remaining bubbles ensure the expulsion of water (*i.e.*, spontaneous dewetting).

Even in these 0.02 μm membranes, the resistance recovery is never 100% because of a number of reasons. First, the contact angle hysteresis is always present, as discussed above: the receding angle can be smaller than the advancing one. Some pores with non-uniform diameter and varying quality of the surface modification do not have sufficient surface tension to effectively expel water. It is unlikely that this effect contributes significantly because of a dramatic change in the pressure between the intrusion and extrusion events and almost an order of magnitude difference in the pore diameters. Second, a hysteresis of surface conductance is similarly present: the sheet resistance, R_s, in eq 1 strongly depends on the density of residual ionizable groups on the surface beneath the hydrophobic layer and was shown to be affected by exposure to water.[13] Third, the processes of water intrusion and expulsion

are not isothermal under our experimental conditions. The membrane resistance in both processes approaches a saturation value very slowly (Figure 3). Water intrusion is an exothermal process because of the work done against the surface tension and condensation of excess water vapor, but more significantly, pressurization of the vessel by gas is also increasing temperature in the chamber. The temperature change needs a significant time to equilibrate with surroundings, which would be seen as a slow component in the resistance decline following the initial sharp drop. The duration of this slow component obviously depends on the change in temperature and the geometry of the cell and the pressurizing chamber. Similarly, the dewetting process is endothermic and is accompanied by the local temperature decline, but the temperature drop due to the nitrogen gas expulsion from the pressure chamber leads to a stronger cooling. As a result, the resistance recovery *via* warming up is slow, as well.

Phenomena similar to those of spontaneous dewetting discussed here are also of importance in designing superhydrophobic/oleophobic surfaces. Combination of the effects of microscopic pockets of air trapped beneath the liquid droplets and the texture of specially engineered surfaces can provide high contact angles with low hysteresis for liquids with greatly varying surface tension.[20,21] In such engineered textures, it is similarly important to have incomplete surface wetting to efficiently support metastable composite solid−liquid−air interfaces.

CONCLUSIONS

We experimentally confirm that long hydrophobic nanopores allow water intrusion under a sufficiently high hydrostatic pressure, the critical value of which depends on the pore diameter and the type/quality of the hydrophobic modification. At the same time, restoring the pressure to the atmospheric one results in spontaneous dewetting *only* when a bubble of vapor is left inside the pore. Such bubbles appear at the regions of narrowing cross section and/or varying quality of the hydrophobic modification and thus can be engineered to control water expulsion. The ionic resistance through the membranes correspondingly demonstrates dramatic changes accompanying these events of electrolyte entering and leaving the pores. The total resistance change spans in excess of 6 orders of magnitude. Recovery of the resistance to the original high value is always less than 100%, which, in addition to the mentioned effects, is due to hysteresis in the conductance of hydrophobic walls after wetting and drying.

MATERIALS AND METHODS

All chemicals used in this work were obtained from Sigma-Aldrich (St Louis, MO) and were used as received.

Three types of free-standing nanoporous alumina membranes were used in this study: commercial "Anodisc" from Whatman (Whatman, Florham Park, NJ) with the nominal 0.2 or 0.02 μm diameter pores (60 μm thick)[11−14] and the homemade 60 μm thick membranes with 70 nm diameter pores. The latter were prepared using a previously described procedure[14] that consists of anodization of cleaned and electropolished Al foil (99.9%, Alfa Aesar, Ward Hill, MA) in oxalic acid at 5 °C and 40 V followed by dissolution of Al substrate in $CuCl_2$ and pore opening/widening in 1 M phosphoric acid at room temperature for 30 min. The membranes were rendered highly hydrophobic using four different modifications (shown in Figure 1), as previously described.[13] In the first scheme, the membrane surface was directly silanized with hexadecyltriethoxysilane from toluene solution (overnight); in the second scheme, the membrane surface was also directly silanized with 1*H*,1*H*,2*H*,2*H*-perfluorooctyltrichlorosilane from toluene solution, also overnight. We will label such membranes as SiH16 and SiH2F6, respectively (see Figure 1). In both cases, the treatment was concluded by thorough washing in ethanol and overnight baking at 120 °C. In the other two schemes, the membrane was first aminated using 3-aminopropyl trimethoxysilane and then carboxylic acid ends of either decanoic acid or 2*H*,2*H*,3*H*,3*H*-perfluoroundecanoic acid were coupled to the surface-bound amino groups using EDC coupling reagent 1-ethyl-3-(3-(dimethylamino)propyl)carbodiimide.[13] We will label such membranes as SiNH9 and SiNH2F8, respectively (see Figure 1). The density of bound to the membrane surface monolayers was monitored by IR absorbance. The data will be presented only for SiH16 and SiNH2F8 modifications because others showed inferior electrical resistance properties compared to these two.[13]

The electrical impedance due to ionic conductance through the membranes was measured in a homemade two-electrode electrochemical cell[13] using a CH 604B electrochemical workstation (from CH Instruments Inc., Austin, TX). The membrane forms a barrier between the two halves of the cell containing degassed 1.0 M potassium chloride in water at pH 7. Two Ag/AgCl electrodes were in close proximity to the membrane, and a low voltage (5 mV) was employed for AC impedance measurements. The open area of the membranes was 0.25 cm^2 that resulted in the resistance of ~17 Ω with unmodified membrane in 1.0 M KCl; that is, this is the minimum measurable resistance or the "cell resistance" under the experimental conditions. The impedance variation with pressure was monitored at 100 Hz. At this frequency, the capacitive contribution to the impedance is minimal. In order to maintain reproducible environment, the cell was first degassed using a water pump and a similarly degassed solution was introduced independently into the both cell compartments by suction. Two 1/8 in. o.d. Tygon tubes were left connected to each side of the cell and filled with electrolyte up to the length of 50 cm. Since gas diffusion through such a long distance is incredibly slow, applying pressure to this assembly hydrostatically with a gas precludes its penetration into the membrane, leaving only electrolyte and water vapor. This assembly was placed inside a homemade stainless steel high-pressure chamber with electrical feed-through contacts for connecting the electrodes to the workstation. The pressure inside the chamber was supplied by nitrogen gas from a tank connected *via* a high-pressure manometer. The maximum controlled pressure was limited by the pressure reductor not to exceed 23 bar above the atmospheric one.

Acknowledgment. This work was partially supported by a grant from the National Science Foundation (NSF DMR 0900238). The authors are also grateful to NM EPSCOR program for providing funds to purchase the potentiostat used in this study.

REFERENCES AND NOTES

1. Lum, K.; Chandler, D.; Weeks, J. Hydrophobicity at Small and Large Length Scales. *J. Phys. Chem. B* **1999**, *103*, 4570–4577.

2. Helmy, R.; Kazakevich, Y.; Ni, C.; Fadeev, A. Wetting in Hydrophobic Nanochannels: A Challenge of Classical Capillarity. *J. Am. Chem. Soc.* **2005**, *127*, 12446–12447.
3. Lum, K.; Chandler, D. Phase Diagram and Free Energies of Vapor Films and Tubes for a Confined Fluid. *Int. J. Thermophys.* **1998**, *19*, 845–855.
4. Lum, K; Luzar, A. Pathway to Surface-Induced Phase Transition of a Confined Fluid. *Phys. Rev. E* **1997**, *56*, R6283–R6286.
5. Luzar, A. Activation Barrier Scaling for the Spontaneous Evaporation of Confined Water. *J. Phys. Chem. B* **2004**, *108*, 19859–19866.
6. Krupenkin, T. N.; Taylor, J. A.; Schneider, T. M.; Yang, S. From Rolling Ball to Complete Wetting: The Dynamic Tuning of Liquids on Nanostructured Surfaces. *Langmuir* **2004**, *20*, 3824–3827.
7. Vlassiouk, I.; Smirnov, S. Biosensing with Nanopores. In *Biosensing Using Nanomaterials*; Merkoci, A., Ed.; Wiley: New York, 2009; pp 459−490.
8. Vlassiouk, I.; Park, C.-D.; Vail, S. A.; Gust, D.; Smirnov, S. Control of Nanopore Wetting by a Photochromic Spiropyran: A Light-Controlled Valve and Electrical Switch. *Nano Lett.* **2006**, *6*, 1013–1017.
9. Rios, F.; Smirnov, S. Biochemically Responsive Smart Surface. *ACS Appl. Mater. Interfaces* **2009**, *1*, 768–774.
10. Holmes-Farley, S. R.; Reamey, R. H.; McCarthy, T. J.; Deutch, J.; Whitesides, G. M. Acid−Base Behavior of Carboxylic Acid Groups Covalently Attached at the Surface of Polyethylene: The Usefulness of Contact Angle in Following the Ionization of Surface Functionality. *Langmuir* **1985**, *1*, 725–740.
11. Hernandez, A.; Martinez, F.; Martin, A.; Pradanos, P. Porous Structure and Surface Charge Density on the Walls of Microporous Alumina Membranes. *J. Colloid Interface Sci.* **1995**, *173*, 284–296.
12. Vlassiouk, I.; Krasnoslobodtsev, A.; Smirnov, S.; Germann, M. 'Direct' Detection and Separation of DNA Using Nanoporous Alumina Filters. *Langmuir* **2004**, *20*, 9913–9915.
13. Smirnov, S.; Vlassiouk, I.; Rios, F.; Vail, S.; Gust, D. Electrical Conductance of Hydrophobic Membranes or What Happens Below the Surface. *Langmuir* **2007**, *23*, 7784–7792.
14. Takmakov, P.; Vlassiouk, I.; Smirnov, S. Application of Anodized Aluminum in Fluorescence Detection of Biological Species. *Anal. Bioanal. Chem.* **2006**, *385*, 954–958.
15. Washburn, E. W. The Dynamics of Capillary Flow. *Phys. Rev.* **1921**, *17*, 273–283.
16. Yu, Y. X.; Gao, G. H.; Li, Y. G. Surface Tension for Aqueous Electrolyte Solutions by the Modified Mean Spherical Approximation. *Fluid Phase Equilib.* **2000**, *173*, 23–38.
17. Lefevre, B.; Saugey, A.; Barrat, J. L.; Bocquet, L.; Charlaix, E.; Gobin, P. F.; Vigier, G. Intrusion and Extrusion of Water in Hydrophobic Mesopores. *J. Chem. Phys.* **2004**, *120*, 4927–4938.
18. Husowitz, B.; Talanquer, V. Nucleation in Cylindrical Capillaries. *J. Chem. Phys.* **2004**, *121*, 8021–8028.
19. Vlassiouk, I.; Takmakov, P.; Smirnov, S. Sensing DNA Hybridization *via* Ionic Conductance through a Nanoporous Electrode. *Langmuir* **2005**, *21*, 4776–4778.
20. Tuteja, A.; Choi, W.; Mabry, J.; McKinley, G.; Cohen, R. Robust Omniphobic Surfaces. *Proc. Natl. Acad. Sci. U.S.A.* **2008**, *105*, 18200–18205.
21. Tuteja, A.; Choi, W.; Ma, M.; Mabry, J.; Mazzella, S.; Rutledge, G.; McKinley, G.; Cohen, R. Designing Superoleophobic Surfaces. *Science* **2007**, *318*, 1618–1622.